Geometrical and Electronic Structure, Stability and Optical Absorption Spectra Comparisons between Thiolate- and Chloride-Stabilized Gold Nanoclusters

Gowri U. Kuda-Singappulige[a] & Christine M. Aikens[a,*]

[a]Department of Chemistry, Kansas State University, Manhattan, KS 66506, USA

[*]cmaikens@ksu.edu, 1-785-532-0954, fax: 1-785-532-6666

Abstract

Thiolate-stabilized gold nanoclusters have drawn significant attention for their extraordinary properties and their applications in many fields such as catalysis, sensing, biomedicine, *etc*. However, due to the size, complexity and conformational flexibility of thiolate ligands, accurate structure prediction can be a challenge using computational approaches. Substitution of thiolate ligands with chloride ligands provides a possible alternative. In this work, the stability of a series of gold thiolate and chloride clusters with 1:1 stoichiometry (Au_nL_n; L=SH, Cl; n=2-9) as well as the analogs of some experimentally observed gold nanoclusters (Au_nL_m; L=SH, Cl; n=18-133) are examined, and binding energies, HOMO-LUMO gaps and absorption spectra are determined using density functional theory (DFT). We observed that the optimized geometries of gold nanoclusters for both types of ligands converged to the same local minimum structure as the experimentally observed structures. The average binding energy per gold atom in gold clusters converges after Au_4L_4. The binding energies of chloride-stabilized gold clusters and nanoclusters average 87.5% and 95.7% of the binding energies of thiolate-stabilized systems for the clusters and nanoclusters, respectively. Typically, thiolates are found to be more stable than the chlorides. However, higher HOMO-LUMO gaps in Au_2Cl_2, $Au_{38}Cl_{24}$, and $Au_{102}Cl_{44}$ compared to their thiolate analogs suggest systems of particular interest for investigating the possible existence of chloride-based gold nanoclusters. Absorption spectra are very similar regardless of the ligand used. This study also demonstrates that in theoretical studies on large nanoclusters, complex thiolate ligands can be replaced by Cl ligands to predict structural and electronic properties with reasonable accuracy and reduced computational effort.

Introduction

Physical and chemical properties of small nanoclusters are generally dissimilar from bulk properties. Nanoscale gold colloids have been used even during ancient times mainly for decoration due to their extraordinary optical properties.[1] In the 21st century, ligand-protected gold nanoclusters that are smaller than 2 nm in core diameter (up to 250 atoms)[1-2] became popular in research areas such as catalysis, bio-imaging, sensing, *etc.*[1, 3-5] because their monodisperse nature assists in the tunability of the optical properties. Gold thiolates are one of the most interesting groups of nanoclusters in this size range; many studies have been performed recently on this group of nanoclusters to understand their structural and electronic properties. The first x-ray crystal structure of an atomically precise gold thiolate nanocluster, a *p*-mercaptobenzoic acid (p-MBA) protected gold cluster consisting of 102 gold atoms and 44 p-MBAs, was characterized by Jadzinsky *et al*. in 2007.[6] Subsequently, other gold thiolate nanoclusters such as $[Au_{25}(SCH_2CH_2Ph)_{18}]^{-1}$ and $Au_{18}(SC_6H_{11})_{14}$ have been synthesized and characterized crystallographically.[7-10] Numerous studies on gold nanocluster structures have been discussed in several recent reviews on atomically precise metal nanoparticles.[5, 11-15]

The electronic structure of gold thiolate clusters can be described by a super atom model that includes the ligand interaction with the gold core.[16] In this representation, the number of valence electrons v of $Au_m(SR)_n^q$ can be calculated by $v = m - n - q$; systems corresponding to noble gas electronic configurations, where the total valence electrons are 2, 8, 18, 34, *etc.*, often show exceptional electronic stability.

Gold thiolate compounds with a 1:1 gold to ligand ratio have been used to treat rheumatoid arthritis[17] and the x-ray structures of the clinically-used compounds such as gold(I) thiomalate (Myochrysine) have been determined.[18] In addition, experimental work on homoleptic gold

thiolate clusters includes the observation of a chair-like structure for $[Au_6S_6(C_{15}H_{23})_6].C_4H_{10}O$ by LeBlanc and Lock[19] and synthesis of catenane structures of $Au_{10}(SC_6H_4$-*p*-$CMe_3)_{10}$ and $Au_{12}(SC_6H_4$-*o*-$CMe_3)_{12}$ by Wiseman *et al*.[20] Using density functional theory (DFT), Grönbeck *et al*. performed a detailed analysis of structural and optical properties of cyclic $(AuSCH_3)_n$ clusters with *n* ranging from 2 to 12.[21] The authors concluded that clusters from $(AuSCH_3)_5$ and above adopt crownlike structures whereas the smaller ones have a planar-ring Au-S framework. They also observed that the electronic structures of gold clusters with different alkyl ligands, $(AuSCH_3)_4$ and $(AuSC_6H_{13})_4$, are similar. Moreover, double helical structures were obtained by Shao and coworkers from their global minimum search on homoleptic gold thiolate clusters $(AuSR)_n$ (n = 6-9).[22] From a theoretical study on gold thiolate clusters, Barngrover and Aikens observed similar formation energies for clusters containing SH and SCH_3 groups, but lower binding energies when phenylthiolate ligands are bound.[23]

DFT has been able to successfully predict structures and choose between isomers of compounds with a large number of electrons as well as high coordination numbers including gold and silver nanoclusters; the benefits of DFT include reasonable accuracy along with less computational cost compared to ab initio methods for these systems.[24-25] However, expanding calculations to predict the structures of larger nanoclusters requires more time and computational resources which in practice limits the cluster size up to several hundred gold atoms. Furthermore, most of the experimentally synthesized thiolate protected nanoclusters possess large ligands such as SCH_2CH_2Ph and SC_6H_{11}, which leads to a huge number of possible isomers and conformers for structure prediction calculations. Therefore, replacing large ligands with small ligands such as SCH_3 and SH is necessary and has been identified as satisfactory in theoretical studies.[23, 26] In a theoretical study of ligand effects and size evolution on the structures and stability of $(AuL)_n$

systems (n = 2 to 13), Liu *et al*. showed the similarity of the structural features of systems with SH ligands to those with SCH_3 ligands, suggesting the possible substitution of SH ligands in $Au_m(SR)_n$ nanoclusters.[26] Using a first principles analysis of $Au_{25}L_{18}^{-1}$ where L is F, Cl, Br, or I, Jiang and Walter noticed that halides, being isoelectronic to thiolate ligands, are a good substitute for thiolates on gold clusters.[27] They showed that the core-staple structure of an all-chloride substituted Au_{25} cluster is a stable local minimum. Halides have been used in other studies as well. Tlahuice-Flores and co-workers employed iso-electronic substitution of thiolate by chloride in icosahedral $Au_{144}(SR)_{60}^{q}$ to determine structural and bonding patterns in the nanocluster.[28] They confirmed from DFT calculations that the *I*-symmetry is held upon replacing thiolate with chloride for the 2+ and 4+ charge states of the nanocluster. The authors further stressed that the high intricacy of solving structural and electronic properties of ligand protected noble metal nanoclusters in this critical size range can be reduced with the isoelectronic method. To the best of our knowledge, chloride analogs of gold thiolate nanoclusters have not yet been synthesized. However, it might be possible that "bare" gold nanoclusters that have been reported[29-31] may actually be stabilized by chloride/bromide ligands, and these clusters could be isolated with modifications in the synthesis such as changing the strength of the reducing agent. Therefore, predicting structures and stability of gold chloride nanoclusters computationally will be beneficial not only for theoretical chemists but also for future experimental studies.

In this work, we compare the stability of a series of isoelectronic and isomorphic gold thiolates and chlorides by means of structure, binding energy, energy gap between the highest occupied molecular orbital (HOMO) and the lowest unoccupied molecular orbital (LUMO), and absorption spectra. In this text, the terms "gold clusters" and "gold nanoclusters" are used to refer to gold compounds with fewer than 250 atoms; "gold clusters" denotes systems containing up to

9 gold atoms while "gold nanoclusters" refers to analogs of known x-ray crystal structures with 18 to 133 gold atoms.

Methodology

Geometries of a series of gold thiolate clusters and their chloride analogs ($(AuL)_n$; n = 2-9, L = SH, Cl) were optimized using DFT. The initial coordinates of the clusters were taken from previous work by Barngrover and Aikens.[23] The simplest thiolate, i.e. -SH, was chosen to compare the stability with chlorides. Another set of structural analogs of recently synthesized gold thiolate nanoclusters, namely $Au_{18}(SR)_{14}$,[9-10] $Au_{20}(SR)_{16}$,[32] $[Au_{23}(SR)_{16}]^-$,[33] $Au_{24}(SR)_{16}$,[34] $Au_{24}(SR)_{20}$,[35] $Au_{24}(SeR)_{20}$,[36] $[Au_{25}(SR)_{18}]^-$,[8] $Au_{28}(SR)_{20}$,[37] $Au_{30}(SR)_{18}$,[38] $Au_{36}(SR)_{24}$,[39] $Au_{38}(SR)_{24}$,[40-41] $Au_{40}(SR)_{24}$,[42] $Au_{44}(SR)_{28}$,[43] $Au_{52}(SR)_{32}$,[42] $Au_{102}(SR)_{44}$,[6] and $Au_{133}(SR)_{52}$,[44] was also examined in terms of stability. Geometry optimizations and linear response time-dependent density functional theory (LR-TDDFT) calculations were performed using the Amsterdam Density Functional (ADF)[45] package with the GGA Becke Perdew (BP86)[46-47] functional and polarized triple - ζ (TZP) frozen core basis set while scalar relativistic effects were included using the zeroth-order regular approximation (ZORA).[48] The self-consistent-field (SCF) convergence criteria was improved to 10^{-8} while changes in energy and gradient during the geometry optimization were tightened to 10^{-5} Hartree and 10^{-4} Hartree/angstrom respectively. The most effective aggressive gradient smoothing was used. The binding energies were calculated based on the reactions presented in equations (1) and (2) for clusters and nanoclusters, respectively. Stabilization energies were calculated using equations (3) and (4) for the clusters and nanoclusters. In equation 4, E_{Au} represents the energy of a free Au atom. Moreover, the average binding energy per gold atom was calculated by dividing the binding energy by the number of gold atoms of the nanocluster.

According to the binding energy calculation, positive binding energies indicate energetically favorable structures.

$$n\,AuL \rightarrow (\mathrm{AuL})_n \quad (1)$$

$$n\,AuL + (m-n)\,Au \rightarrow Au_mL_n \quad (2)$$

$$E_{binding,clusters} = n\,E_{AuL} - E_{(AuL)_n} \quad (3)$$

$$E_{binding,nanoparticles} = n\,E_{AuL} + (m-n)\,E_{Au} - E_{Au_mL_n} \quad (4)$$

A large energy difference between the highest occupied molecular orbital (HOMO) and the lowest unoccupied molecular orbital (LUMO) also contributes to the stability of a compound.[49] Li and coworkers reported that tetrahedral Au_{20} cluster shows a HOMO-LUMO gap of 1.8 eV, which is about 0.2 eV greater than that of C_{60}, by photoelectron spectroscopy as well as by density functional calculations.[50] We also calculate the HOMO-LUMO gap of the clusters and nanoclusters of interest in this work for further comparison of their stability.

Absorption spectra of SH and Cl analogs of experimentally available clusters up to $Au_{102}L_{44}$ were calculated using LR-TDDFT implemented in the ADF package using the same computational accuracy used for the optimization unless otherwise mentioned. In order to simplify the calculations for the $Au_{102}L_{44}$ system, a double - ζ (DZ) frozen core basis set was used. The lowest 200 transitions were calculated for all nanoclusters up to $Au_{44}L_{28}$; $Au_{52}L_{32}$ and larger systems required up to 800 states to get excitations up to at least 2 eV. The excitations were convoluted with a Gaussian function with a 0.2 eV full width at half maximum value.

Results and Discussion

Optimized Structures

The optimized structures of gold clusters Au_nL_n and gold nanoclusters Au_nL_m are shown in Figures 1 and 2, respectively. The average Au-S and Au-Cl bond lengths of cyclic clusters are approximately 2.4 Å for both ligands. S-Au-S and Au-S-Au bond angles are approximately 174° and 93° whereas the corresponding values for gold chlorides are 175° and 86°. Similar values have been observed experimentally and theoretically by Bau,[18] LeBlanc and Lock,[19] Wiseman *et al.*,[20] Grönbeck *et al.*,[21] and Barngrover and Aikens.[23]

The two isomeric structures of $Au_{24}L_{20}$ (1) and (2) are the structural analogs of $Au_{24}(SCH_2Ph\text{-}^tBu)_{20}$ from Das *et al.*[35] and a selenolate-capped structure, $Au_{24}(SeC_6H_5)_{20}$, from Song *et al.*[36] respectively. The structure of $Au_{38}(SR)_{24}$ with the face-fused biicosahedral Au_{23} core reported by Qian *et al.*[40] is represented by $Au_{38}L_{24}$ (1) and a less stable structural isomer synthesized by Tian and co-workers[41] is labeled as $Au_{38}L_{24}$ (2). The geometries of the optimized nanoclusters for both types of ligands converged with the same local minimum structures as the synthesized crystal structures. For example, both thiolate and chloride protected $Au_{18}L_{14}$ are composed of an Au_9 kernel surrounded by one Au_4L_5 tetramer, one Au_2L_3 dimer and three AuL_2 monomers.[9-10]

It should be noted that it has previously been observed that the core sizes of nanoclusters protected by bulky or aromatic thiols can vary significantly from those of alkylthiolate-protected gold nanoclusters.[51-55] However, theoretical work suggests that the electronic structure of cyclic thiolates with alkylthiolate ligands is similar[21] and that the alkylthiolate ligands can be further

reduced to -SH groups for structure prediction of $Au_n(SR)_m$ compounds.[23, 26] The current work demonstrates the similarities between chloride-protected and alkylthiolate-protected gold clusters and nanoclusters.

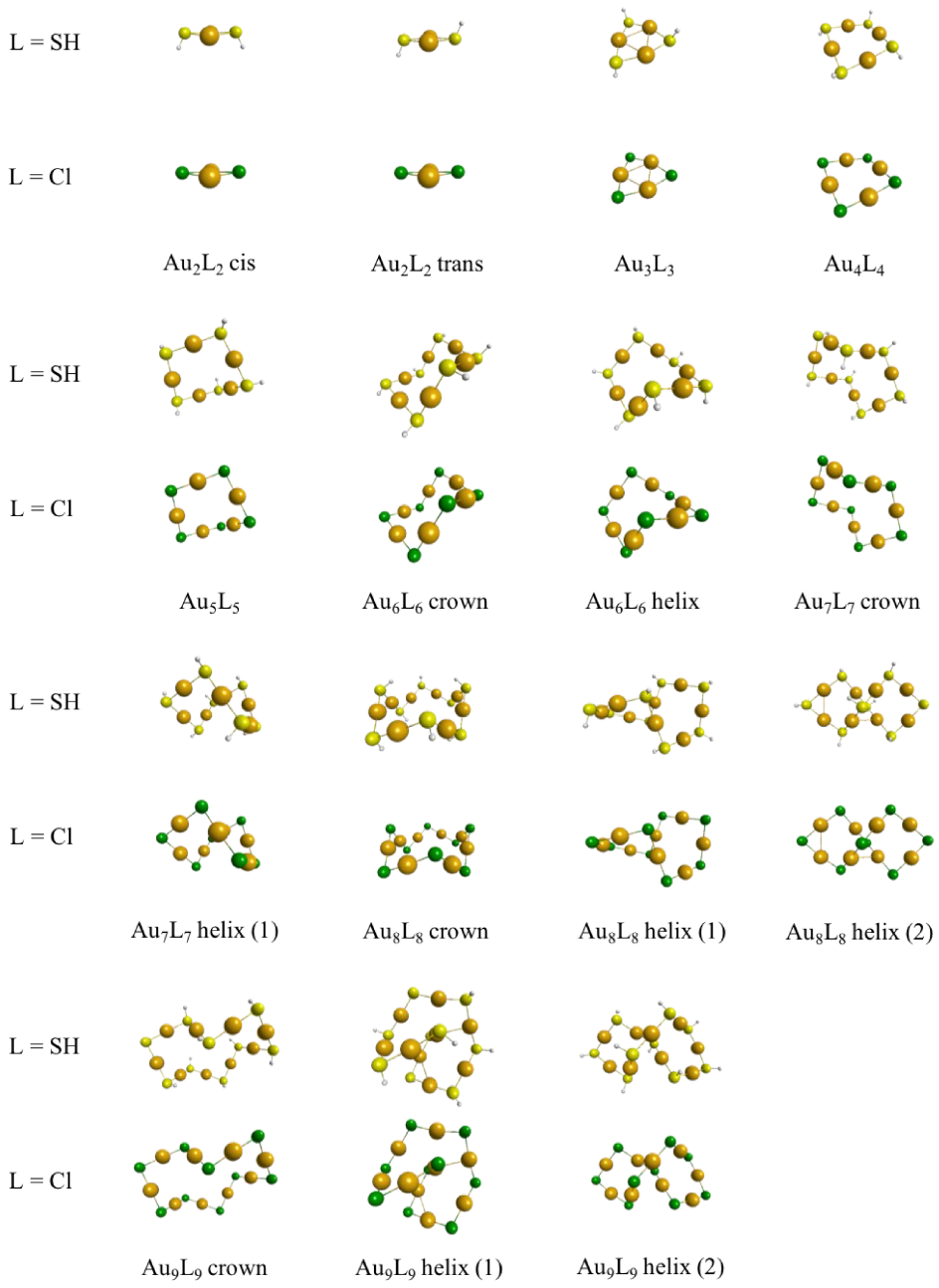

Figure 1. Optimized gold thiolate and gold chloride clusters $(AuL)_n$ (n = 2-9). Key: Au: gold, S: yellow, H: white, Cl: green.

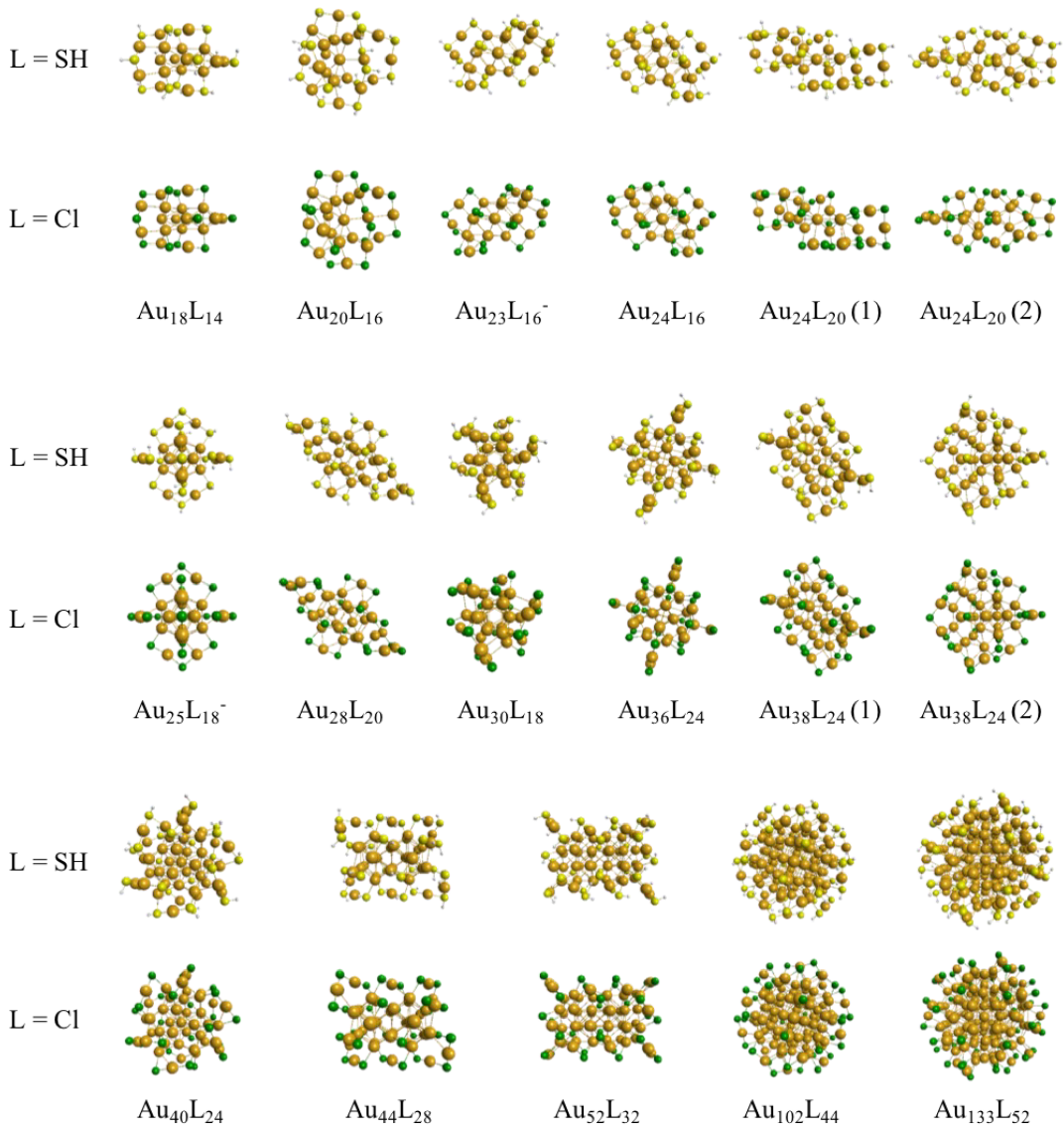

Figure 2. Optimized gold thiolate and gold chloride nanoclusters Au_nL_m.

Molecular orbitals (MOs) (isosurface = 0.03) of $(AuL)_2$ and $(AuL)_4$ with thiolate and chloride ligands are compared in Figure 3. Clusters with two gold atoms (Figure 3a) clearly manifest similarity between the MOs for the SH and Cl ligands. Both thiolate and chloride stabilized clusters share the same contributions of atomic orbitals (AOs) that contribute to a particular MO. For example, gold 5d and sulfur (or chlorine for the chloride analog) 3p are the primary AOs contributing to the HOMO of $(AuL)_2$. However, it may not be clear at first glance

that this similarity still remains for the MOs of $(AuL)_4$ (Figure 3b). As the cluster size gets larger, there are many occupied orbitals with very similar energy, and the degeneracy of the MOs with the size of the clusters leads to different linear combinations of AOs for an individual orbital. Nevertheless, the formation of the frontier orbitals from a combination of gold 5d and 6s with 3p of sulfur/chlorine is consistent for all gold clusters. The similarity in MOs is not restricted to the smaller gold clusters. The frontier MOs of the larger nanoclusters are also qualitatively insensitive to whether thiolate or chloride ligands are used. The frontier orbitals of $Au_{18}L_{14}$ are shown in Figure 4 (isosurface = 0.02). Again, these orbitals appear the same regardless of the protecting ligand. Note that here we show the similarity between the -SH and -Cl ligated gold nanoclusters; aliphatic (alkylthiolate) ligands are expected to resemble these ligands whereas the bulky and/or aromatic ligands may show different structural and electronic properties from those of alkylthiolates.

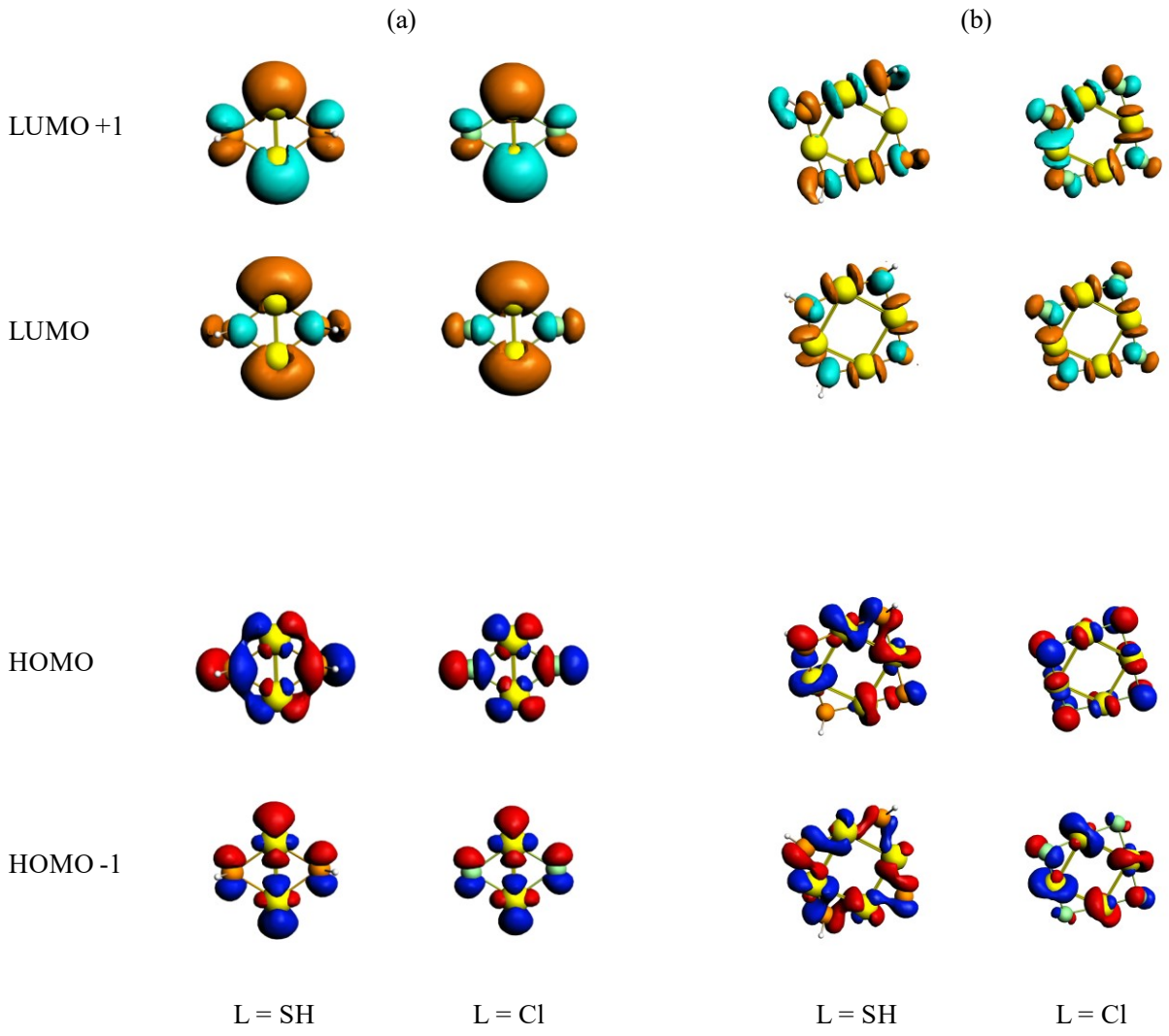

Figure 3. Frontier molecular orbitals of (a) $(AuL)_2$ and (b) $(AuL)_4$. Color code: Red and blue indicate opposite phases of occupied orbitals, whereas orange and cyan denote opposite phases of unoccupied orbitals.

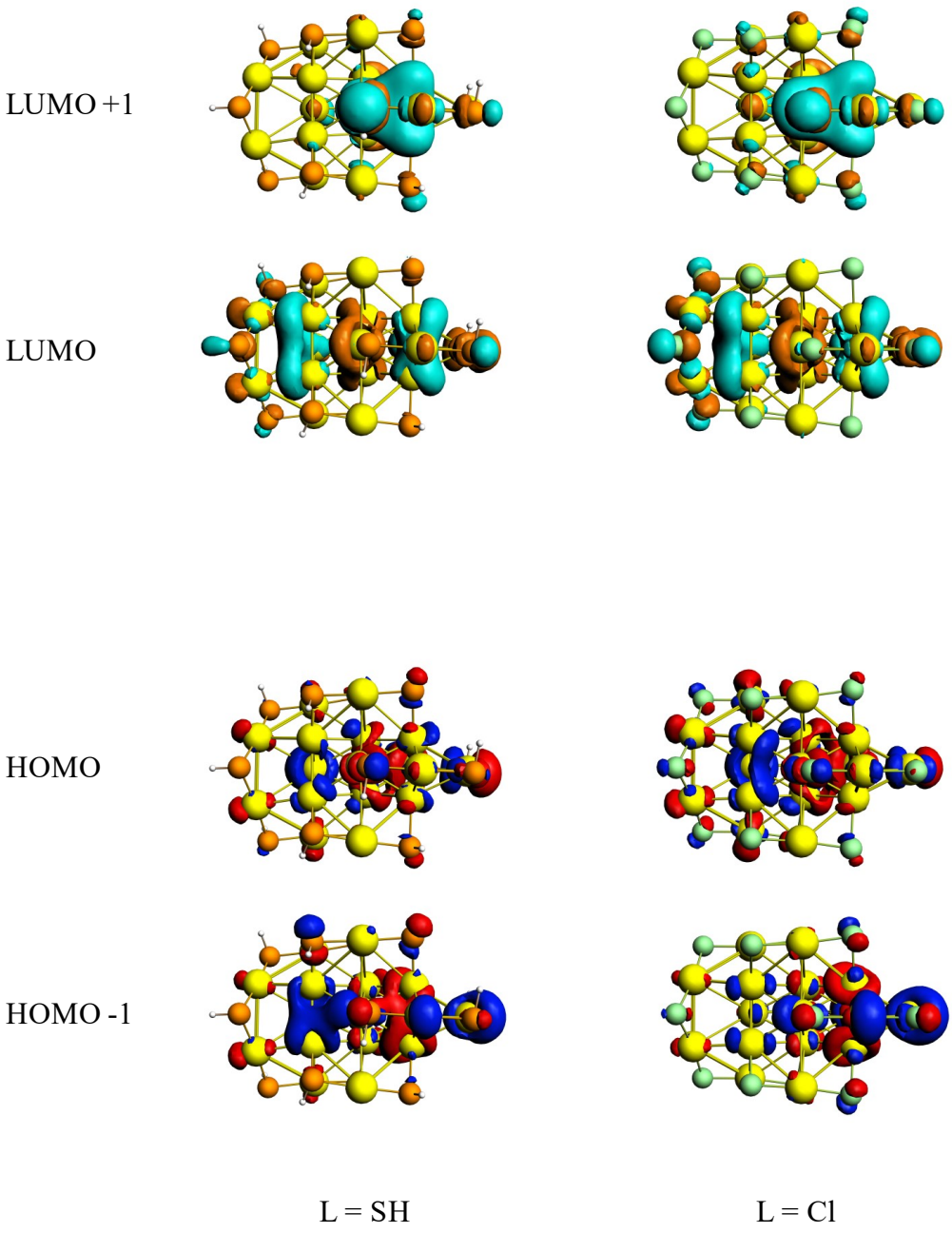

Figure 4. Frontier molecular orbitals of $Au_{18}L_{14}$. Color code: Red and blue indicate opposite phases of occupied orbitals, whereas orange and cyan denote opposite phases of unoccupied orbitals.

Binding Energy

As indicated in Figure 5, total binding energies, calculated using equation 3, increase with the size of the gold-thiolate cluster, and isomers with the same stoichiometry have almost the same binding energy (Table S1). Steric strain in the $(AuL)_2$ and $(AuL)_3$ clusters is thought to be responsible for the lower stability of these systems.[21, 23] As evidenced by the positive binding energies, it can be noticed that chloride ligands also favorably form gold clusters. The ratio between the binding energies of gold chlorides to those of thiolates varies around an average of 87.5% (±0.6) for these systems (Table 1). Moreover, average binding energies per gold atom converge after four gold atoms in both thiolates and chlorides (Figure 6). This result is in agreement with previous work.[21, 23, 26] In addition, average binding energies of the cyclic clusters with SH ligands are similar to the average binding energies of cyclic methyl thiolate gold clusters calculated by Barngrover[23] using the same exchange-correlation functional (BP86) (Table 1). This supports the idea that the complexity of theoretical calculations can be simplified by replacing SCH_3 groups with SH as suggested by previous work.[23, 26]

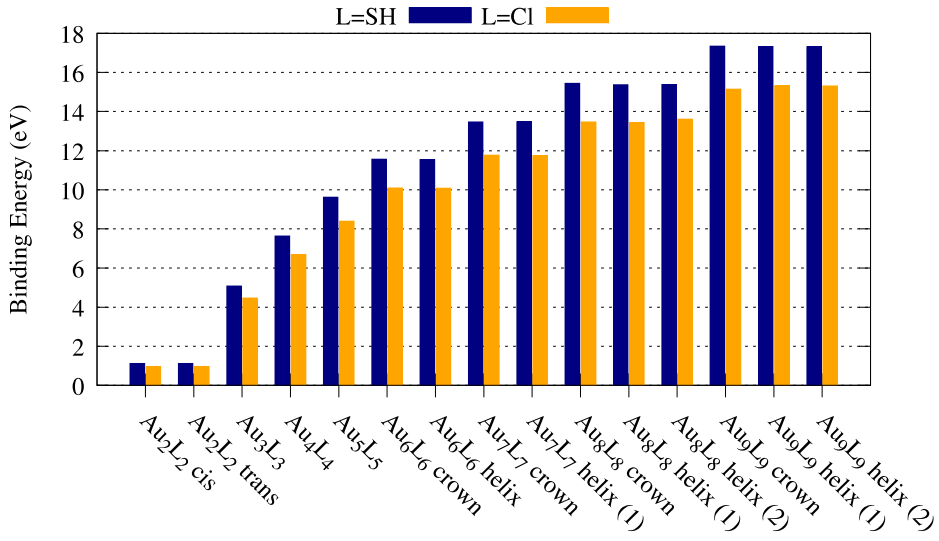

Figure 5. Total binding energies of gold clusters.

Table 1. Average binding energies per gold atom of small cyclic thiolate and chloride gold clusters and the ratio between the average binding energies for Cl and SH species.

Cluster	**L=SH (eV)**	**L=Cl (eV)**	**L=SCH_3 (eV) (ref [23])**	**Cl:SH (%)**
Au_2L_2 cis	0.56	0.48	0.54	86.5
Au_2L_2 trans	0.55	0.48	0.55	86.9
Au_3L_3	1.69	1.49	1.69	88.0
Au_4L_4	1.91	1.67	1.91	87.5
Au_5L_5	1.92	1.68	1.92	87.3
Au_6L_6 crown	1.93	1.68	1.92	87.3
Au_6L_6 helix	1.92	1.68	1.92	87.3
Au_7L_7 crown	1.92	1.68	1.92	87.3
Au_7L_7 helix (1)	1.93	1.68	1.92	87.1
Au_7L_7 helix (2) [a]	1.92	1.68	1.92	87.4
Au_8L_8 crown	1.93	1.68	1.92	87.2
Au_8L_8 helix (1)	1.92	1.68	1.92	87.5
Au_8L_8 helix (2)	1.92	1.70	1.93	88.5
Au_9L_9 crown	1.93	1.68	1.91	87.4
Au_9L_9 helix (1)	1.93	1.70	1.92	88.4
Au_9L_9 helix (2)	1.92	1.70	1.93	88.4

[a] Both SH and Cl structures of Au_7L_7 helix (2) were converged to crown geometry

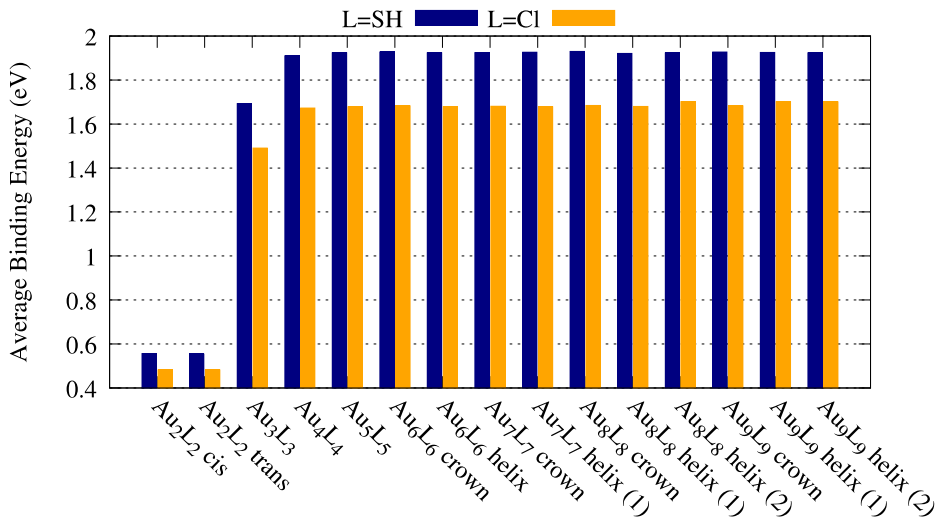

Figure 6. Average binding energies per gold atom of gold clusters.

A similar analysis was carried out with the gold nanoclusters. Binding energies of both chloride and thiolate stabilized nanoclusters are positive (Figure 7 and Table S2); thiolates are more stable, but the difference is relatively small and tends to decrease with the size of the nanocluster. When going from $Au_{52}L_{32}$ to $Au_{102}L_{44}$, the binding energy almost doubles because the size also essentially doubles. In consequence, it is useful to consider the average binding energies, as defined by equation (4). While the average binding energy per gold atom converged at around 1.9 eV and 1.7 eV in cyclic clusters with thiolate and chloride ligands respectively (Table 1 and Figure 6), the average binding energy of nanoclusters varies around 2.1 eV (Table 2 and Figure 8). Binding energies of chlorides are approximately 95.7% (±1.7) of the binding energy of thiolates. This average ratio is higher than that for gold clusters due to the larger size and the composition of the nanoclusters. The nanoclusters have Au-Au bonds with bonding energies that effectively do not change depending on the ligand, which causes the similarity of average binding energies for the two ligands. Because of the consistent ratio between binding energies, one could

use the average ratio along with the binding energy results for computed chloride-stabilized nanoclusters to predict the binding energies of novel thiolate-stabilized gold nanoclusters.

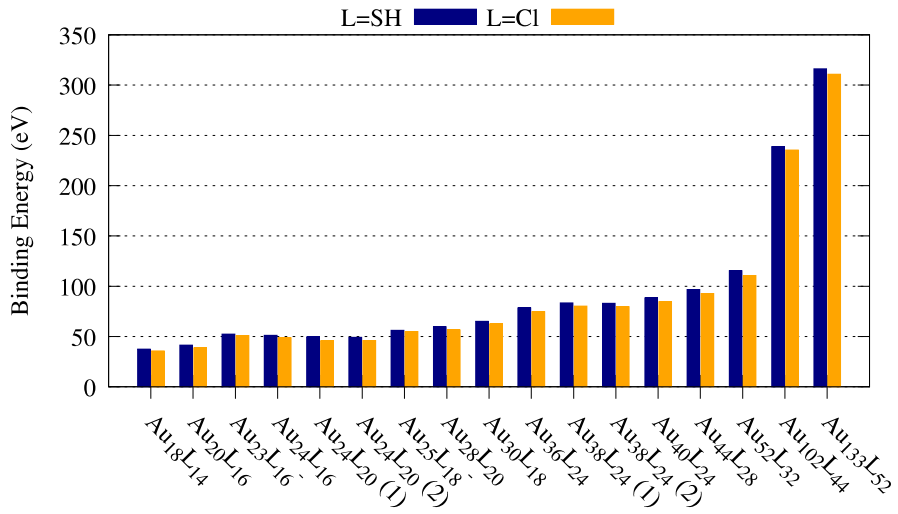

Figure 7. Total binding energies of gold nanoclusters.

Table 2. Average binding energies per gold atom of gold nanoclusters and the ratio between the average binding energies for Cl and SH species.

Nanocluster	**Average binding energy per Au (L=SH) /eV**	**Average binding energy per Au (L=Cl) /eV**	**Cl:SH (%)**
$Au_{18}L_{14}$	2.08	1.97	94.9
$Au_{20}L_{16}$	2.07	1.93	93.2
$Au_{23}L_{16}^{-}$	2.28	2.22	97.4
$Au_{24}L_{16}$	2.13	2.03	94.9
$Au_{24}L_{20}$ (1)	2.07	1.91	92.4
$Au_{24}L_{20}$ (2)	2.05	1.92	93.4
$Au_{25}L_{18}^{-}$	2.25	2.20	97.7
$Au_{28}L_{20}$	2.14	2.02	94.5
$Au_{30}L_{18}$	2.17	2.08	95.9
$Au_{36}L_{24}$	2.18	2.07	95.2

$Au_{38}L_{24}$ (1)	2.19	2.11	96.3
$Au_{38}L_{24}$ (2)	2.19	2.10	95.9
$Au_{40}L_{24}$	2.21	2.12	95.9
$Au_{44}L_{28}$	2.20	2.11	95.8
$Au_{52}L_{32}$	2.22	2.13	95.9
$Au_{102}L_{44}$	2.34	2.31	98.6
$Au_{133}L_{52}$	2.38	2.34	98.3

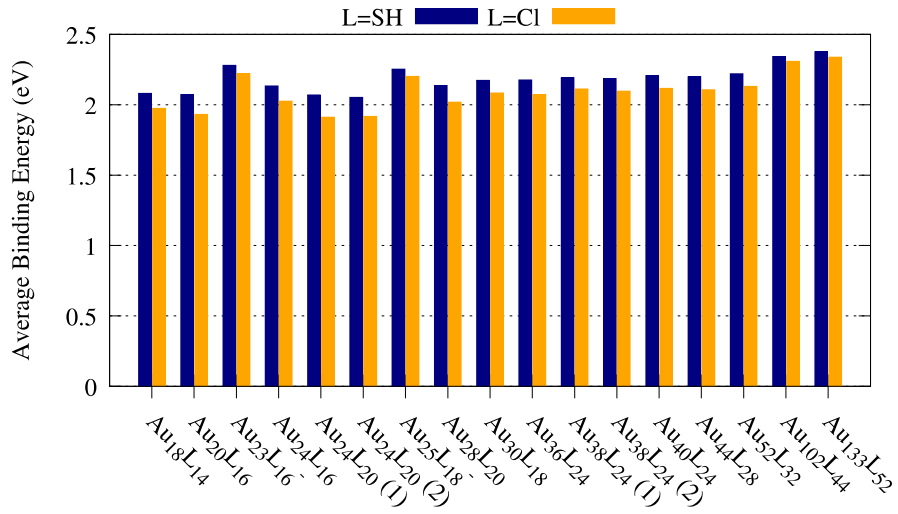

Figure 8. Average binding energies per gold atom of gold nanoclusters.

HOMO – LUMO Gap

It is known that the HOMO-LUMO gap generally decreases with increasing size. Nanoclusters in the size range < 2 nm show an enhanced HOMO-LUMO gap and high stability compared to larger nanoclusters.[56-57] However, the electronic stability is controlled by several factors such as the type of ligand, geometric arrangement of the staple motifs and the symmetry of the core.[16, 21] Herein we compare the stability of thiolate- and chloride-stabilized nanoclusters in terms of their HOMO-LUMO gaps. For the small cyclic clusters as well as larger nanoclusters,

thiolates have a larger HOMO-LUMO gap than chlorides (Figures 9 and 10; Tables S3 and S4) except for a few systems, suggesting higher electronic stability. In the two cis- and trans- Au_2L_2 clusters, Cl makes the cluster more stable, which may be due to electronic effects or to a lesser steric hindrance compared to SH. Among the nanoclusters, $Au_{102}L_{44}$ and the most stable isomer of $Au_{38}L_{24}$ are predicted to have larger HOMO-LUMO gaps in chloride-stabilized systems compared to the thiolate versions (Figure 10 and Table S4). This implies that it may be valuable to study these chloride compounds further to determine whether it is possible to synthesize atomically precise chloride-stabilized systems if appropriate synthesis conditions (reducing agent, *etc*.) are used.

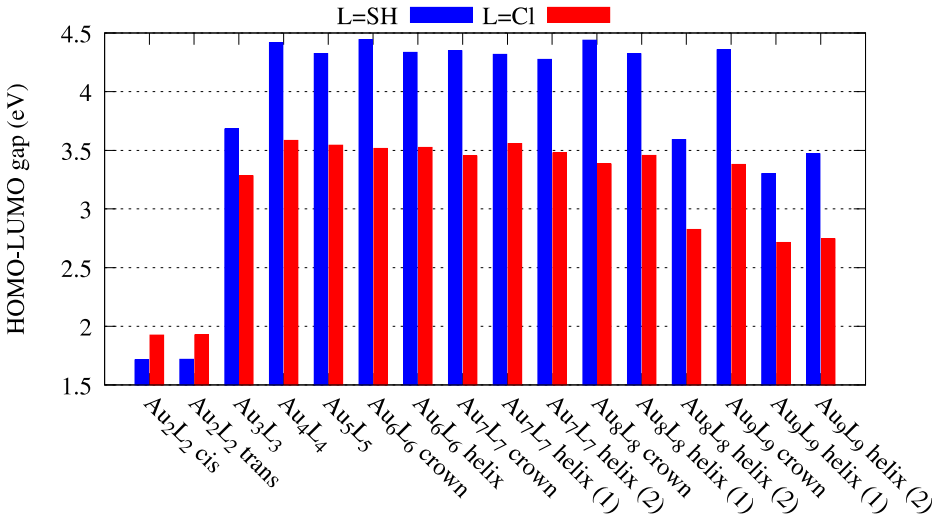

Figure 9. HOMO – LUMO gaps of gold clusters.

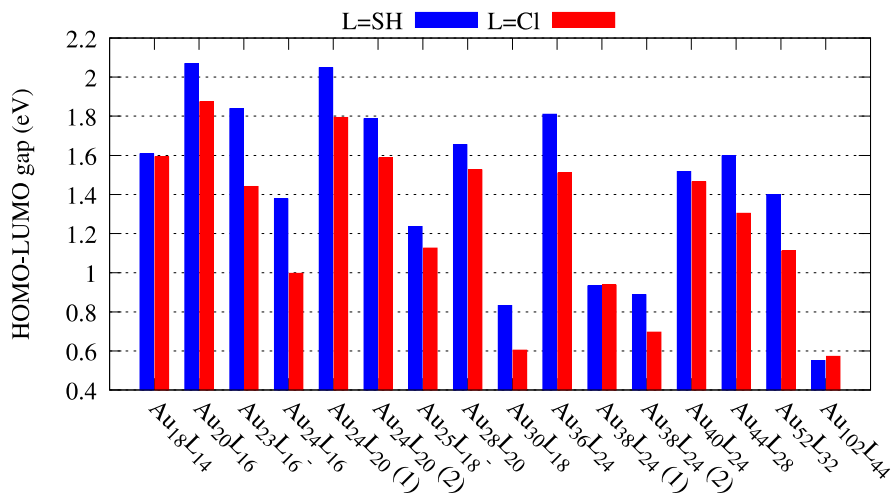

Figure 10. HOMO – LUMO gaps of gold nanoclusters.

Absorption Spectra

The shape of the absorption spectra of chloride-stabilized nanoclusters are generally similar to those of the corresponding SH-passivated clusters with a redshift of peak positions. Spectra for $Au_{18}L_{14}$, $Au_{25}L_{18}^-$, and $Au_{102}L_{44}$ are shown in Figure 11; the others are provided in Figure S1. Since the electronic transitions correspond to the energies in the UV/vis region, we are interested in the lower energy end of the spectrum. (Note that the sudden drop at the UV end does not necessarily imply that a peak reaches a maximum before the drop; the spectrum falls simply because there are no more excited states calculated.) When the system size increases, the energy range that can be calculated becomes narrower for a constant number of states.

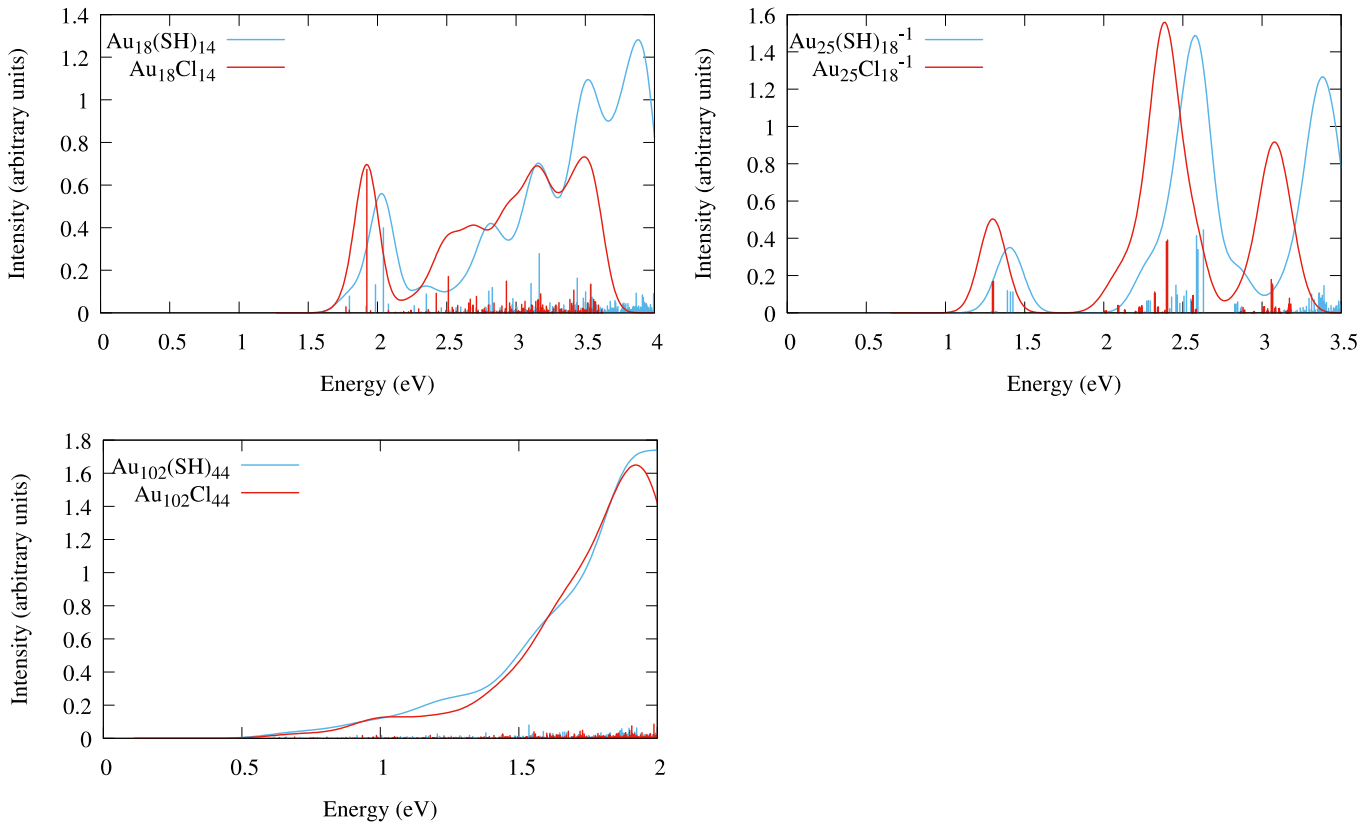

Figure 11. Absorption spectra of selected nanoclusters. (Note: The sudden drop at the UV end does not necessarily imply that a peak reaches a maximum before the drop; the spectrum falls due to the finite number of excited states calculated.)

The lowest energy peak of $Au_{18}L_{14}$ appears at around 1.8 eV in both ligands, which can be compared with the experimentally observed peak position that occurs near 1.97 eV (~630 nm) by Das *et al.*[10] and Chen *et al.*[9] in the $Au_{18}(SC_6H_{11})_{14}$ nanocluster. Even though the transition from HOMO to LUMO orbitals is the prominent contribution for this peak in the SH based nanocluster (Tables S5 and S6), similar to the previous work of Das and co-workers,[10] a somewhat weaker transition from HOMO-1 to LUMO appears to destructively cancel the oscillator strength in the lowest energy transition. Similarly, the HOMO → LUMO and HOMO-1 → LUMO transitions in the chloride nanocluster couple with each other in a destructive fashion (Tables S7 and S8). We

also observe a prominent peak at 2.0 eV and 1.9 eV in thiolate and chloride protected nanoclusters respectively, which is comparable with the experimental value of 2.18 eV (570 nm)[9-10]. We found that the HOMO → LUMO and HOMO-1→ LUMO transitions constructively add to give rise to these excitations regardless of the type of ligand attached to the nanocluster. Overall, for both thiolates and chlorides the two transitions from HOMO to LUMO and LUMO+1 destructively and constructively couple to generate a lower and a higher energy excitation respectively.

It is clear from this spectral transition analysis that systems ligated with chlorides would bear qualitatively similar transition properties to those ligated by thiolates. Numerical variances may arise due to the difference in the HOMO-LUMO gap and as a result of raising the symmetry of the chloride-stabilized systems compared to the thiolate clusters, which affects the orbital energy levels (Figure S2). For example, the energy levels of the frontier orbitals of $Au_{18}Cl_{14}$ shift towards lower energy compared to $Au_{18}(SH)_{14}$ (Table S9). In the Cl-based nanocluster, the frontier virtual orbitals are more stabilized compared to the occupied orbitals, leading to a lowering of the energy gap and the corresponding excitation energies. Frontier molecular orbitals are composed of Au and S/Cl atomic orbitals in both types of gold nanoclusters, and the ligand contributions to the frontier orbitals appear to be similar in both chloride and thiolate analogues. However, for higher energy virtual orbitals, we observe that more ligand-based orbitals (arising from S and H atomic orbitals) are present in the thiolate cluster whereas the contributions from the Cl atoms to these orbitals is less in the chloride version. Overall, it can be concluded that the spectra of chloride- and thiolate-protected gold nanoclusters are very similar up to the point where the ligand effects start to contribute at higher energy.

The spectra of $Au_{25}L_{18}$ show clear comparison for the Cl and SH ligated nanoclusters. The three main peaks of the SH-stabilized nanocluster at 1.4, 2.6 and 3.4 eV have been redshifted to

1.3, 2.4, and 3.1 eV in Cl-stabilized nanoclusters. The red shifts of the excitation energies of chloride-ligated structures arise due to the lower HOMO-LUMO gaps of chloride-stabilized systems compared to thiolates. Moreover, the spectrum of $Au_{25}Cl_{18}$ is narrower than $Au_{25}SH_{18}$ due to the fact that the Cl systems can achieve slightly higher symmetry. For instance, the three distinct excitations near 1.3 eV in the spectrum of $Au_{25}Cl_{18}$ are closer in energy compared to the corresponding excitations of $Au_{25}SH_{18}$ at around 1.4 eV. The high symmetry induces degeneracy in the electronic structure leading to degenerate excitations. To this end, substitution of thiolates with isoelectronic chlorides helps achieve high symmetry and increases the computational efficiency for potential structure and property predictions.

For $Au_{102}L_{44}$, the spectra almost overlap for the two ligands. Calculation of excitations up to 2 eV for the Cl ligand captures one of the two shoulder-like peaks around 2 eV shown in spectrum of $Au_{102}(SH)_{44}$. Moreover, structure in the optical absorption spectrum around 1-1.2 eV is captured for both ligands. Again, the chloride-stabilized nanocluster exhibits a spectrum that is slightly red-shifted compared to the thiolate-stabilized system because the Cl-stabilized system experiences increased stabilization of its frontier virtual orbitals compared to its occupied orbitals.

Conclusion

Atomic and electronic structures, binding energies, average binding energies, HOMO-LUMO gaps, and absorption spectra of thiolate- and chloride-stabilized gold clusters and nanoclusters were compared in this study. The gold core of optimized gold nanoclusters converged to the same structure as the experimentally determined structures for both thiolate and chloride ligands. The binding energy increases with the size of the cluster and isomers tend to have similar binding energies in both thiolate and chloride stabilized gold clusters. Calculated average binding energies of $(AuSH)_n$ are similar to the previously reported average binding energies of $(AuSCH_3)_n$

where the same level of theory was employed. Calculated average binding energies per gold atom converge after Au_4L_4 in the gold clusters with a 1:1 gold to ligand ratio. Binding energies of chloride-stabilized gold clusters are about 87.5% (±0.6) of those of thiolate-stabilized systems; the corresponding average ratio for gold nanoclusters is found to be 95.7% (±1.7). Even though the binding energies and average binding energies of chloride gold clusters are numerically smaller than those of thiolate gold clusters, they are still predicted to be stable, just as the thiolate-stabilized systems are, and can be considered as a potential alternative to thiolates. Generally, thiolates have higher HOMO-LUMO gaps than chlorides except for Au_2L_2, $Au_{38}L_{24}$ (1), and $Au_{102}L_{44}$. The spectra are very similar regardless of ligand, with the chloride-stabilized systems exhibiting peaks at slightly lower energy that may be somewhat sharper due to a higher overall symmetry in the nanocluster compared to thiolate-stabilized systems. Overall, the binding energy, HOMO-LUMO gap, and excitation spectra results suggest that chlorides may provide a possible ligand that could be employed experimentally, and strongly suggest that theoretical studies aimed at structural predictions could effectively employ chloride ligands.

Acknowledgement

This material is based on work supported by the National Science Foundation under Grant No. CHE-1507909. The computing for this project was performed on the Beocat Research Cluster at Kansas State University, which is funded in part by NSF Grants CHE-1726332, CNS-1006860, EPS-1006860, and EPS-0919443.

Supporting Information Available

Binding energies and HOMO-LUMO gaps of gold cluster and nanoclusters. Absorption spectra of gold nanoclusters. Orbital energy level diagram of $Au_{18}(SH)_{14}$ and $Au_{18}Cl_{14}$. Energies

and oscillator strengths of the first four excited states of $Au_{18}(SH)_{14}$ and $Au_{18}Cl_{14}$. Occupied-unoccupied orbital transitions, their weights, and their contributions to the transition dipole moment of excited states 1 and 4 of $Au_{18}(SH)_{14}$ and $Au_{18}Cl_{14}$. Comparison of molecular orbital energies of $Au_{18}(SH)_{14}$ and $Au_{18}Cl_{14}$.

References

1. Jin, R., Quantum Sized, Thiolate-Protected Gold Nanoclusters. *Nanoscale* **2010,** *2* (3), 343-362.

2. Cleveland, C. L.; Landman, U.; Schaaff, T. G.; Shafigullin, M. N.; Stephens, P. W.; Whetten, R. L., Structural Evolution of Smaller Gold Nanocrystals: The Truncated Decahedral Motif. *Phys. Rev. Lett.* **1997,** *79* (10), 1873-1876.

3. Daniel, M. C. M.; Astruc, D., Gold Nanoparticles: Assembly, Supramolecular Chemistry, Quantum-Size Related Properties and Applications toward Biology, Catalysis and Nanotechnology. *Chem. Rev.* **2004,** *104*, 293-346.

4. Cobley, C. M.; Chen, J.; Cho, E. C.; Wang, L. V.; Xia, Y., Gold Nanostructures: A Class of Multifunctional Materials for Biomedical Applications. *Chem. Soc. Rev.* **2011,** *40* (1), 44-56.

5. Jin, R.; Zeng, C.; Zhou, M.; Chen, Y., Atomically Precise Colloidal Metal Nanoclusters and Nanoparticles: Fundamentals and Opportunities. *Chem. Rev.* **2016,** *116* (18), 10346-10413.

6. Jadzinsky, P. D.; Calero, G.; Ackerson, C. J.; Bushnell, D. A.; Kornberg, R. D., Structure of a Thiol Monolayer-Protected Gold Nanoparticle at 1.1 Å Resolution. *Science* **2007,** *318* (5849), 430-433.

7. Heaven, M. W.; Dass, A.; White, P. S.; Holt, K. M.; Murray, R. W., Crystal Structure of the Gold Nanoparticle $[N(C_8H_{17})_4][Au_{25}(SCH_2CH_2Ph)_{18}]$. *J. Am. Chem. Soc.* **2008,** *130* (12), 3754-3755.

8. Zhu, M.; Aikens, C. M.; Hollander, F. J.; Schatz, G. C.; Jin, R., Correlating the Crystal Structure of A Thiol-Protected Au_{25} Cluster and Optical Properties. *J. Am. Chem. Soc.* **2008,** *130* (18), 5883-5885.

9. Chen, S.; Wang, S.; Zhong, J.; Song, Y.; Zhang, J.; Sheng, H.; Pei, Y.; Zhu, M., The Structure and Optical Properties of the [$Au_{18}(SR)_{14}$] Nanocluster. *Angew. Chem., Int. Ed.* **2015,** *54* (10), 3145-3149.

10. Das, A.; Liu, C.; Byun, H. Y.; Nobusada, K.; Zhao, S.; Rosi, N.; Jin, R., Structure Determination of [$Au_{18}(SR)_{14}$]. *Angew. Chem., Int. Ed.* **2015,** *54* (10), 3140-3144.

11. Ma, Z.; Wang, P.; Xiong, L.; Pei, Y., Thiolate-Protected Gold Nanoclusters: Structural Prediction and the Understandings of Electronic Stability from First Principles Simulations. *Wiley Interdiscip. Rev. Comput. Mol. Sci.* **2017,** *7* (4), e1315/1-19.

12. Zhang, J.; Li, Z.; Zheng, K.; Li, G., Synthesis and Characterization of Size-Controlled Atomically Precise Gold Clusters. *Phys. Sci. Rev.* **2018,** *3* (10), 20170083/1-29.

13. Kang, X.; Zhu, M., Intra-Cluster growth Meets Inter-Cluster Assembly: The Molecular and Supramolecular Chemistry of Atomically Precise Nanoclusters. *Coord. Chem. Rev.* **2019,** *394*, 1-38.

14. Ni, T. W.; Tofanelli, M. A.; Ackerson, C. J., Structure Determination by Single-Crystal X-Ray Crystallography. In *Protected Metal Clusters: From Fundamentals to Applications*, Häkkinen, H.; Tsukuda, T., Eds. Elsevier: 2015; Vol. 9, pp 103-125.

15. Chakraborty, I.; Pradeep, T., Atomically Precise Clusters of Noble Metals: Emerging Link between Atoms and Nanoparticles. *Chem. Rev.* **2017,** *117* (12), 8208-8271.

16. Walter, M.; Akola, J.; Lopez-Acevedo, O.; Jadzinsky, P. D.; Calero, G.; Ackerson, C. J.; Whetten, R. L.; Grönbeck, H.; Häkkinen, H., A Unified View of Ligand-Protected Gold Clusters as Superatom Complexes. *Proc. Natl. Acad. Sci. U.S.A.* **2008,** *105* (27), 9157-9162.

17. Elder, R. C.; Eidsness, M. K., Synchrotron X-ray Studies of Metal-Based Drugs and Metabolites. *Chem. Rev.* **1987,** *87* (5), 1027-1046.

18. Bau, R., Crystal Structure of the Antiarthritic Drug Gold Thiomalate (Myochrysine): A Double-Helical Geometry in the Solid State. *J. Am. Chem. Soc.* **1998,** *120* (36), 9380-9381.

19. LeBlanc, D. J.; Lock, C. J. L., *cyclo*-Hexakis[(2,4,6-triisopropylthiophenolato-*S*:*S*)gold(I)] Diethyl Ether Solvate. *Acta. Crystallogr. C.* **1997,** *53* (12), 1765-1768.

20. Wiseman, M. R.; Marsh, P. A.; Bishop, P. T.; Brisdon, B. J.; Mahon, M. F., Homoleptic Gold Thiolate Catenanes. *J. Am. Chem. Soc.* **2000,** *122* (50), 12598-12599.

21. Grönbeck, H.; Walter, M.; Häkkinen, H., Theoretical Characterization of Cyclic Thiolated Gold Clusters. *J. Am. Chem. Soc.* **2006,** *128* (31), 10268-10275.

22. Shao, N.; Pei, Y.; Gao, Y.; Zeng, X. C., Onset of Double Helical Structure in Small-Sized Homoleptic Gold Thiolate Clusters. *J. Phys. Chem. A* **2009,** *113* (4), 629-632.

23. Barngrover, B. M.; Aikens, C. M., Incremental Binding Energies of Gold(I) and Silver(I) Thiolate Clusters. *J. Phys. Chem. A* **2011,** *115* (42), 11818-11823.

24. Aikens, C. M., Modelling Small Gold and Silver Nanoparticles with Electronic Structure Methods. *Molecular Simulation* **2012,** *38* (8-9), 607-614.

25. Weerawardene, K. L. D. M.; Häkkinen, H.; Aikens, C. M., Connections Between Theory and Experiment for Gold and Silver Nanoclusters. *Ann. Rev. Phys. Chem.* **2018,** *69* (1), 205-229.

26. Liu, Y.; Tian, Z.; Cheng, L., Size Evolution and Ligand Effects on the Structures and Stability of $(AuL)_n$ (L = Cl, SH, SCH_3, PH_2, $P(CH_3)_2$, n = 1-13) Clusters. *RSC Adv.* **2016,** *6* (6), 4705-4712.

27. Jiang, D.-e.; Walter, M., The Halogen Analogs of Thiolated Gold Nanoclusters. *Nanoscale* **2012,** *4* (14), 4234-4239.

28. Tlahuice-Flores, A.; Black, D. M.; Bach, S. B. H.; Jose-Yacamán, M.; Whetten, R. L., Structure & Bonding of the Gold-Subhalide Cluster I-$Au_{144}Cl_{60}^{[z]}$. *Phys. Chem. Chem. Phys.* **2013,** *15* (44), 19191-19195.

29. Fink, J.; Kiely, C. J.; Bethell, D.; Schiffrin, D. J., Self-Organization of Nanosized Gold Particles. *Chem. Mater.* **1998,** *10* (3), 922-926.

30. Brust, M.; Walker, M.; Bethell, D.; Schiffrin, D. J.; Whyman, R., Synthesis of Thiol-Derivatised Gold Nanoparticles in a Two-Phase Liquid–Liquid System. *ChemComm* **1994,** (7), 801-802.

31. Petroski, J.; Chou, M.; Creutz, C., The Coordination Chemistry of Gold Surfaces: Formation and Far-infrared Spectra of Alkanethiolate-capped Gold Nanoparticles. *J. Organomet. Chem.* **2009,** *694* (7), 1138-1143.

32. Zeng, C.; Liu, C.; Chen, Y.; Rosi, N. L.; Jin, R., Gold–Thiolate Ring as a Protecting Motif in the $Au_{20}(SR)_{16}$ Nanocluster and Implications. *J. Am. Chem. Soc.* **2014,** *136* (34), 11922-11925.

33. Das, A.; Li, T.; Nobusada, K.; Zeng, C.; Rosi, N. L.; Jin, R., Nonsuperatomic $[Au_{23}(SC_6H_{11})_{16}]^-$ Nanocluster Featuring Bipyramidal Au_{15} Kernel and Trimeric $Au_3(SR)_4$ Motif. *J. Am. Chem. Soc.* **2013,** *135* (49), 18264-18267.

34. Crasto, D.; Barcaro, G.; Stener, M.; Sementa, L.; Fortunelli, A.; Dass, A., $Au_{24}(SAdm)_{16}$ Nanomolecules: X-ray Crystal Structure, Theoretical Analysis, Adaptability of Adamantane Ligands to Form $Au_{23}(SAdm)_{16}$ and $Au_{25}(SAdm)_{16}$, and its Relation to $Au_{25}(SR)_{18}$. *J. Am. Chem. Soc.* **2014,** *136* (42), 14933-14940.

35. Das, A.; Li, T.; Li, G.; Nobusada, K.; Zeng, C.; Rosi, N. L.; Jin, R., Crystal Structure and Electronic Properties of a Thiolate-protected Au_{24} Nanocluster. *Nanoscale* **2014,** *6* (12), 6458-6462.

36. Song, Y.; Wang, S.; Zhang, J.; Kang, X.; Chen, S.; Li, P.; Sheng, H.; Zhu, M., Crystal Structure of Selenolate-Protected $Au_{24}(SeR)_{20}$ Nanocluster. *J. Am. Chem. Soc.* **2014,** *136* (8), 2963-2965.

37. Zeng, C.; Li, T.; Das, A.; Rosi, N. L.; Jin, R., Chiral Structure of Thiolate-Protected 28-Gold-Atom Nanocluster Determined by X-ray Crystallography. *J. Am. Chem. Soc.* **2013,** *135* (27), 10011-10013.

38. Higaki, T.; Liu, C.; Zeng, C.; Jin, R.; Chen, Y.; Rosi, N. L.; Jin, R., Controlling the Atomic Structure of Au_{30} Nanoclusters by a Ligand-Based Strategy. *Angew. Chem. Int. Ed.* **2016,** *55* (23), 6694-6697.

39. Nimmala, P. R.; Knoppe, S.; Jupally, V. R.; Delcamp, J. H.; Aikens, C. M.; Dass, A., $Au_{36}(SPh)_{24}$ Nanomolecules: X-ray Crystal Structure, Optical Spectroscopy, Electrochemistry, and Theoretical Analysis. *J. Phys. Chem. B* **2014,** *118* (49), 14157-14167.

40. Qian, H.; Eckenhoff, W. T.; Zhu, Y.; Pintauer, T.; Jin, R., Total Structure Determination of Thiolate-Protected Au_{38} Nanoparticles. *J. Am. Chem. Soc.* **2010,** *132* (24), 8280-8281.

41. Tian, S.; Li, Y.-Z.; Li, M.-B.; Yuan, J.; Yang, J.; Wu, Z.; Jin, R., Structural Isomserism in Gold Nanoparticles Revealed by X-ray Crystallography. *Nat. Commun.* **2015,** *6*, 8667/1-6.

42. Zeng, C.; Chen, Y.; Liu, C.; Nobusada, K.; Rosi, N. L.; Jin, R., Gold Tetrahedra Coil Up: Kekulé-Like and Double Helical Superstructures. *Sci. Adv.* **2015,** *1* (9), e1500425/1-6.

43. Zeng, C.; Chen, Y.; Iida, K.; Nobusada, K.; Kirschbaum, K.; Lambright, K. J.; Jin, R., Gold Quantum Boxes: On the Periodicities and the Quantum Confinement in the Au_{28}, Au_{36}, Au_{44}, and Au_{52} Magic Series. *J. Am. Chem. Soc.* **2016,** *138* (12), 3950-3953.

44. Zeng, C.; Chen, Y.; Kirschbaum, K.; Appavoo, K.; Sfeir, M. Y.; Jin, R., Structural Patterns at all Scales in a Nonmetallic Chiral $Au_{133}(SR)_{52}$ Nanoparticle. *Sci. Adv.* **2015,** *1* (2), e1500045/1-6.

45. te Velde, G.; Bickelhaupt, F. M.; Baerends, E. J.; Fonseca Guerra, C.; van Gisbergen, S. J. A.; Snijders, J. G.; Ziegler, T., Chemistry with ADF. *J. Comput. Chem.* **2001,** *22* (9), 931-967.

46. Perdew, J. P., Density-Functional Approximation for the Correlation Energy of the Inhomogeneous Electron Gas. *Phys. Rev. B* **1986,** *33* (12), 8822-8824.

47. Becke, A. D., Density-Functional Exchange-Energy Approximation with Correct Asymptotic Behavior. *Phys. Rev. A.* **1988,** *38* (6), 3098-3100.

48. van Lenthe, E.; Ehlers, A.; Baerends, E.-J., Geometry Optimizations in the Zero Order Regular Approximation or Relativistic Effects. *J. Chem. Phys.* **1999,** *110* (18), 8943-8953.

49. Häkkinen, H., Atomic and Electronic Structure of Gold Clusters: Understanding Flakes, Cages and Superatoms from Simple Concepts. *Chem. Soc. Rev.* **2008,** *37* (9), 1847-1859.

50. Li, J.; Li, X.; Zhai, H.-J.; Wang, L.-S., Au_{20}: A Tetrahedral Cluster. *Science* **2003,** *299* (5608), 864-867.

51. Price, R. C.; Whetten, R. L., All-Aromatic, Nanometer-Scale, Gold-Cluster Thiolate Complexes. *J. Am. Chem. Soc.* **2005,** *127* (40), 13750-13751.

52. Nimmala, P. R.; Dass, A., $Au_{36}(SPh)_{23}$ Nanomolecules. *J. Am. Chem. Soc.* **2011,** *133* (24), 9175-9177.

53. Krommenhoek, P. J.; Wang, J.; Hentz, N.; Johnston-Peck, A. C.; Kozek, K. A.; Kalyuzhny, G.; Tracy, J. B., Bulky Adamantanethiolate and Cyclohexanethiolate Ligands Favor Smaller Gold Nanoparticles with Altered Discrete Sizes. *ACS Nano* **2012,** *6* (6), 4903-4911.

54. Nishigaki, J.-i.; Tsunoyama, R.; Tsunoyama, H.; Ichikuni, N.; Yamazoe, S.; Negishi, Y.; Ito, M.; Matsuo, T.; Tamao, K.; Tsukuda, T., A New Binding Motif of Sterically Demanding Thiolates on a Gold Cluster. *J. Am. Chem. Soc.* **2012,** *134* (35), 14295-14297.

55. Crasto, D.; Dass, A., Green Gold: $Au_{30}(S\text{-}t\text{-}C_4H_9)_{18}$ Molecules. *J. Phys. Chem. C* **2013,** *117* (42), 22094-22097.

56. Murray, R. W., Nanoelectrochemistry: Metal Nanoparticles, Nanoelectrodes, and Nanopores. *Chem. Rev.* **2008,** *108* (7), 2688-2720.

57. Nimmala, P. R.; Yoon, B.; Whetten, R. L.; Landman, U.; Dass, A., $Au_{67}(SR)_{35}$ Nanomolecules: Characteristic Size-Specific Optical, Electrochemical, Structural Properties and First-Principles Theoretical Analysis. *J. Phys. Chem. A* **2013,** *117* (2), 504-517.

TOC Graphic